

# Structural and optical properties of ZnS:Mn micro-powders, synthesized from the charge with a different Zn/S ratio

Yu. Yu. Bacherikov<sup>1</sup> · N. P. Baran<sup>1</sup> · I. P. Vorona<sup>1</sup> · A. V. Gilchuk<sup>2</sup> · A. G. Zhuk<sup>1</sup> · Yu. O. Polishchuk<sup>1</sup> · S. R. Lavorik<sup>1</sup> · V. P. Kladko<sup>1</sup> · S. V. Kozitskii<sup>3</sup> · E. F. Venger<sup>1</sup> · N. E. Korsunskaya<sup>1</sup>

Received: 11 November 2016 / Accepted: 14 February 2017 / Published online: 27 February 2017  
© Springer Science+Business Media New York 2017

**Abstract** The influence of Zn/S ratio in the charge on structural and optical properties of ZnS:Mn powders produced by high-temperature self-propagated synthesis was investigated. The samples were shown to consist of mixed-polytypes ZnS crystallites with hexagonal (2H) and cubic (3C) phases, the contribution of the latter increases with the sulfur content in the charge. The most homogeneous size distribution was found at stoichiometric Zn/S ratio. The Zn/S relation affects the Mn incorporation into ZnS lattice. The highest quantity of incorporated Mn is observed at stoichiometric Zn/S relation while lowest one is realized at Zn excess. Besides, the distribution of manganese ions in the blocks, which compose the crystallites, was found to be inhomogeneous, their concentration decreases from crystallites surface to the depth. Mn ions are nearer to the surface in ZnS:Mn synthesized with Zn excess. At Mn concentration in the charge of 1 wt% the shift of ZnS band edge to low energy side is observed, that is ascribed to formation of solid solution ZnS–MnS with lower band gap value.

## 1 Introduction

ZnS is one of the widely studied materials due to its emission properties (photoluminescence and

electroluminescence) allowing its applications as the base materials for electronic and optoelectronic devices (in particular, flat panel displays [1, 2]). To obtain the emission of different colors a number of impurities were introduced into ZnS. One of the important impurities in zinc sulfide is manganese. So, the Mn-doped ZnS, including the micro- and nano-powders, is important and intensively studied material [3–8]. A great attention has been paid to development of cheap and simple methods for preparation of doped ZnS. One of the effective and low-cost methods for production of various industrially useful materials is the method of self-propagated high-temperature synthesis (SHS), enabling the doping in the process of crystal growth. Though SHS is known for a long time it is modified until now [9] resulting in change of synthesized crystal properties. Note, that some properties of ZnS crystals grown by both conventional and modified SHS techniques including structure and impurities incorporation are unclear.

SHS technique is characterized by some features such as non-equilibrium conditions of crystal growth accompanied by the rapid cooling of grown crystals, formation of a great number of extended defects as well as the specific composition of the surface layer of growing crystal. This can affect the crystal structure and impurity incorporation.

In the most cases of materials growth by SHS the wave of structure formation follows the wave of chemical conversions [10]. Due to this, the chemical reaction between Zn and S takes place not only in the combustion front but also in the molten zone of these components [11, 12]. The extent of reaction depends on pressure value in reactor, the cooling rate, the presence of impurity and other factors. For example, in the case of high cooling rate the degree of component reaction is  $\approx 60\%$  only. The mentioned factors result in the different forms of crystal growth (layer-wise or dendritic). In [13, 14] it is assumed, that the main reason

✉ Yu. Yu. Bacherikov  
yuyu@isp.kiev.ua

<sup>1</sup> V.E. Lashkaryov Institute of Semiconductor Physics NAS of Ukraine, 45 Nauky ave, Kyiv 03028, Ukraine

<sup>2</sup> National Technical University of Ukraine «Kyiv Polytechnic Institute», 37 Pobedy ave, Kyiv 03506, Ukraine

<sup>3</sup> Odessa National Maritime Academy, 8, Didrikhson str., Odessa 65029, Ukraine

of dendritic form of crystal growth in SHS method is the presence of impurities in the melt. It is supposed, that they are ejected to the surface during crystal growth or adsorbed on it and can serve as the nucleation centers for new crystallite growth [13]. At the same time, in [15] the homogeneous Mn impurity distribution in ZnS crystals grown by SHS is claimed.

On the other hand, the properties of grown crystals including structure and impurity incorporation may depend on the components ratio in the charge. Such dependence was observed in ZnSe:Mn nanocrystals grown by organometallic synthesis [16]. It was shown that the highest incorporated Mn content took place under excess of Se that can be caused by the higher binding energy of the impurity to the surface of the nanocrystal [16] or the lower energy of impurity formation [17]. However, for the powders grown by SHS, this was not investigated. At the same time, the mentioned above features can influence the impurity incorporation.

In fact, in the case of SHS the composition of the surface layer of growing crystal is governed by reactions which are specific for this method. The mechanisms and macro kinetics of reactions under combustion were investigated in [15, 18]. It was concluded that during crystallization process the formation of  $Zn_{x-1}S_x$  solid solution boundary layer around the stoichiometric ZnS grains takes place. This layer has the lower melting temperatures than that of stoichiometric ZnS and appears due to incorporation of atoms from liquid phase to solid one. This causes the specific conditions of crystal surface formation.

In this work the dependence of Mn incorporation and its distribution in ZnS crystals on Zn/S ratio in the charge as well as the influence of Zn/S on crystal structure (cubic or hexagonal) and crystallite size distribution were investigated by XRD, SEM, EPR, diffuse reflectance and photoluminescence methods.

## 2 Experiment details

Powdered ZnS:Mn was produced by SHS method from a charge containing Zn, S and  $MnCl_2$  in nitrogen atmosphere. Three series of samples were studied. For samples labeled as ZnS:Mn, sulfur and zinc in the charge were taken in stoichiometric ratio. Samples of the second series labeled as ZnS(Zn):Mn were synthesized with zinc excess (of about 10%), and samples of the third group ZnS(S):Mn were grown with sulfur excess (~10%). Mn ion impurity concentration in all cases was 1 wt%.

X-ray diffraction was studied with the powder diffractometer ARL X'TRA ( $CuK\alpha$  wavelength  $\lambda=0.15418$  nm). The coherent domain size was evaluated by the Scherrer formula  $D_{hkl}=0.9\lambda/\beta_{hkl}\cos\theta$ , where  $\lambda$ —wavelength,

$\beta_{hkl}$ —the full width at half maximum of the reflex,  $\theta$ —the angular position of the peak.

The morphology and particle size distribution in synthesized powders were examined by scanning electron microscopy (SEM) in a secondary electron mode using JAMP 9500F (Jeol, Japan) microscope. Powder for analysis was placed into a graphite adhesive and applied on the copper substrate. The following characteristics were selected for analysis: probe current 0.1 nA, the accelerating voltage –30 kV. Processing of the electron micrographs was performed using Image-Pro Plus package. Statistics was performed by size of smaller rectangles drawn around the sides of the particles (minimum Feret diameter), and also by squares for particles in electron micrographs.

EPR spectra were recorded with the X-band spectrometer “Varian E12” at room temperature. In order to avoid distortions of the EPR lines, small power (<2 mW) of microwave and amplitude modulation of the magnetic field 0.1 mT were used. To quantify the number of paramagnetic centers, experiments were performed using a paired cavity that allows recording EPR signals from standard (MgO:Mn with  $3\times 10^{15}$  centers) and studied samples separately by modulation switching.

Diffuse reflectance spectra were recorded with respect to the  $BaSO_4$  standard on double-beam spectrophotometer UV-3600 UV-Vis NIR made by Shimadzu company, equipped with an integrated sphere ISR-3100.

The photoluminescence (PL) and luminescence excitation (PLE) spectra were recorded at room temperature using SDL-2 device. The excitation of samples was carried out by the light of xenon lamp DKSSh-150 through a MDR-12 monochromator (low excitation level) or by the light of nitrogen laser LGI-21 ( $\lambda=337$  nm) (high excitation level).

## 3 Results and discussion

### 3.1 Structural characteristics

#### 3.1.1 Morphology and particle size distribution

Figures 1 and 2 shows the original micrographs as well as statistics on the particle size and percentage of space occupied by them. Particle size distribution approximated by lognormal functions is shown in Fig. 2. Histograms of area percentage, occupied by particles of a specific size range, were approximated by Gaussian distribution. The most probable values of the particle size ( $d_0$ ), average size ( $d$ ), and the particle size which corresponds to the largest part of the micrographs area ( $d_c$ ), are given in Table 1.

As it can be seen from these results, the highest values of the most probable particle size are observed in the

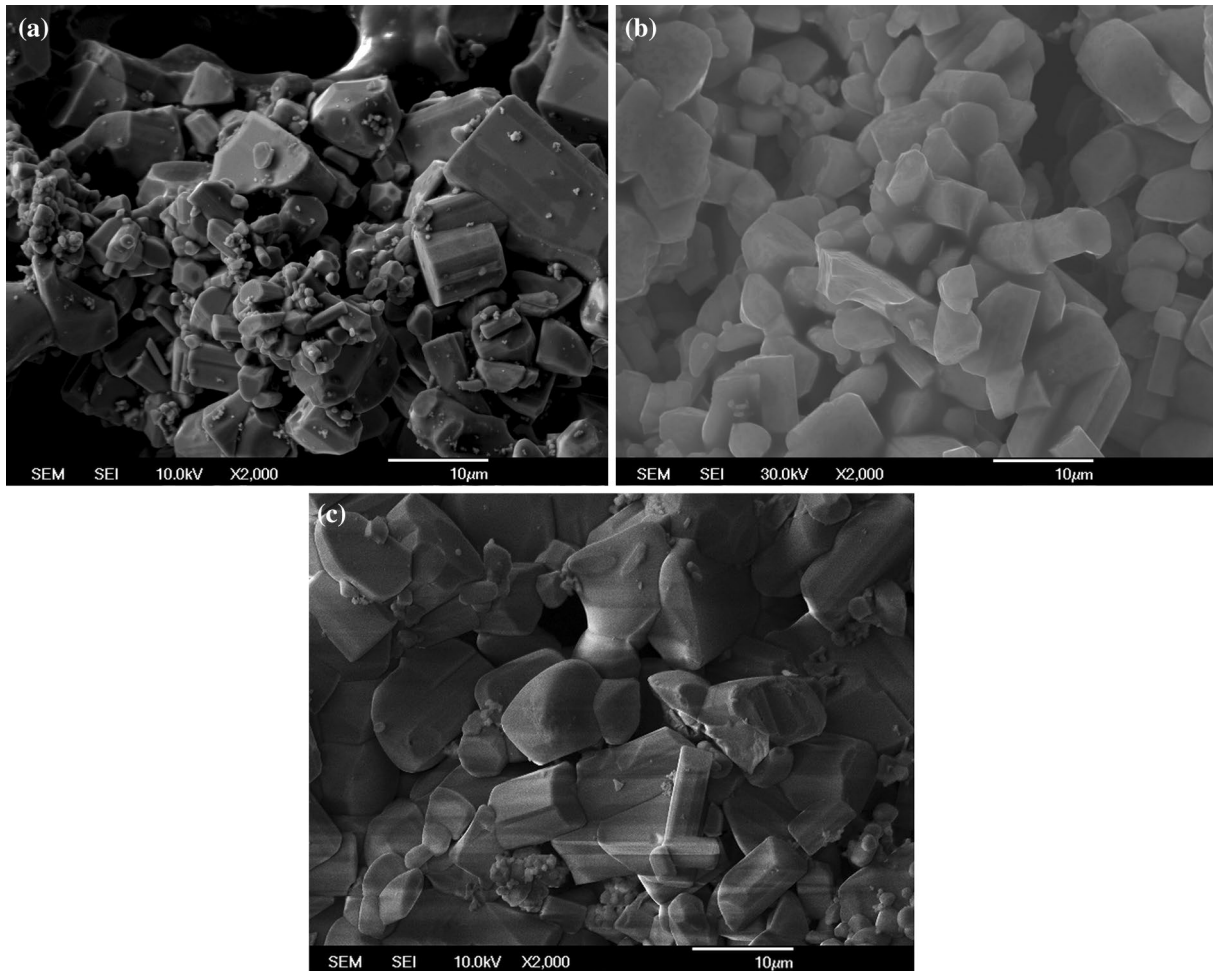


**Fig. 1** Powder micrographs ZnS(S):Mn (a), ZnS:Mn (b) и ZnS(Zn):Mn (c)

ZnS:Mn samples, obtained with the stoichiometric Zn/S ratio in the charge. There is also observed a more uniform size distribution (Fig. 1). At the same time, ZnS(S):Mn and ZnS(Zn):Mn powders have both large and very small particles. The average and the most probable size of the particles in ZnS(Zn):Mn is larger than in ZnS(S):Mn. It should be noted that the size of particles with a maximum area is larger than their average size. This means that the main volume of the resulting material is concentrated in the larger particles. The size of these particles is maximal in ZnS(Zn):Mn powder. This is in agreement with the shift of homogeneity region of Zn–S system to Zn side. At the same time the appearance of high enough number of small crystallites can be caused by nonequilibrium grows condition.

### 3.1.2 XRD

XRD patterns of all the samples show the presence of ZnS hexagonal and cubic phases, hexagonal phase being

dominant (Fig. 3). The dependence of the ratio of phase contribution on the charge composition is given in Table 1. The presence of other phases in the samples was not found. As it can be seen from Table 1, the increase of the Zn/S ratio without the change of manganese content (1%), leads to the decrease of the relative contribution of cubic phases. This is consistent with the work [15]. At the same time, the coherent domain size in hexagonal phase does not depend substantially on the charge composition. Evaluation of  $D$  for the cubic phase is not possible because of the weakness of the corresponding reflections.

As it can be seen from the Table 1, the particle size, determined from electron microscopy data, significantly larger than  $D$  value. This means that obtained microcrystals have the block structure.

### 3.1.3 EPR

The EPR spectra of all samples (shown in Fig. 4) are the superposition of the two signals—a complex

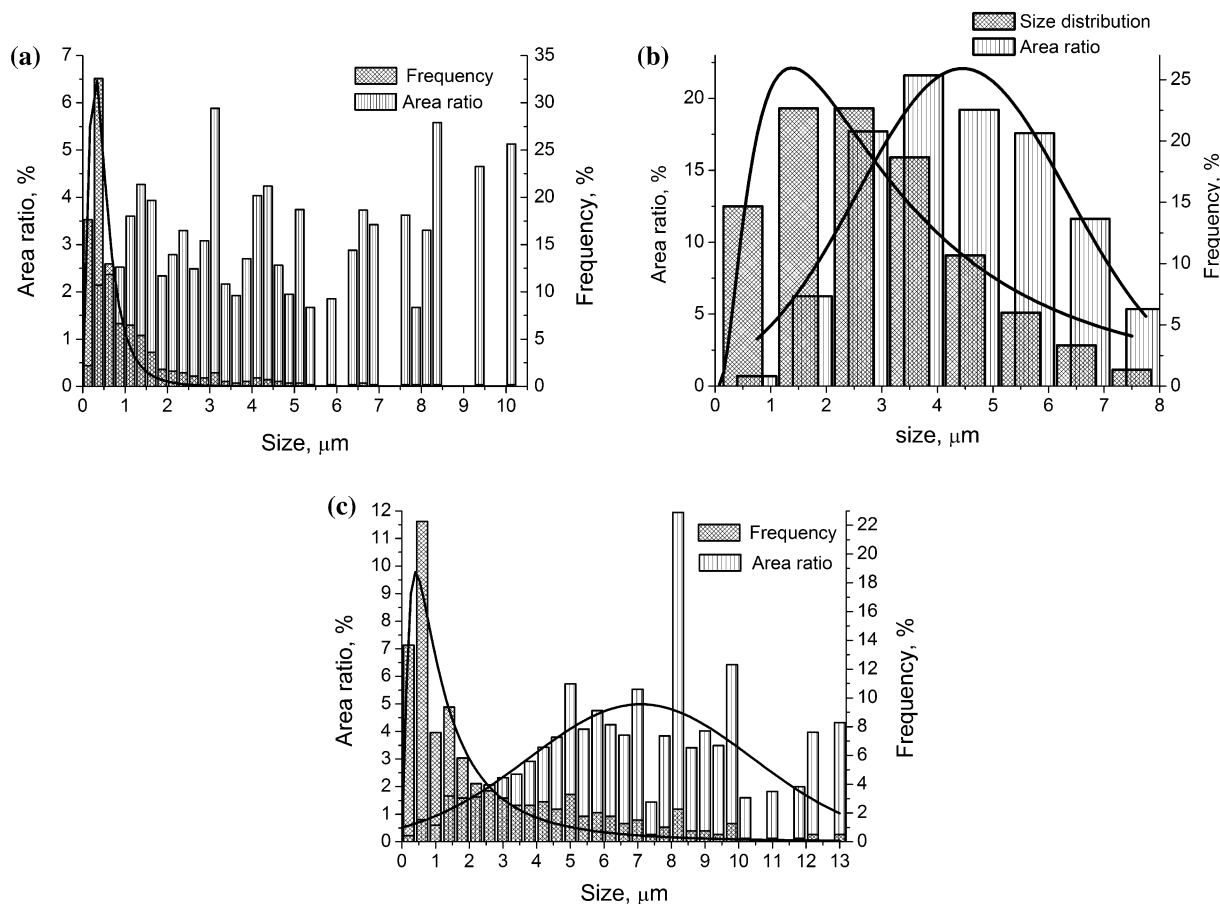


**Fig. 2** Statistics on the particle size and area of specific size particles in ZnS(S):Mn (a), ZnS:Mn (b), ZnS(Zn):Mn (c)

**Table 1** Structural parameters of ZnS:Mn powders

Sample parameter	SEM data			XRD data	
	$d_0$ ( $\mu\text{m}$ )	$d$ ( $\mu\text{m}$ )	$d_s$ ( $\mu\text{m}$ )	$D$ (nm)	Phase ratio ZnS (Cub./Hex.)
ZnS(S):Mn	$0.34 \pm 0.02$	$0.44 \pm 0.02$	–	53–62	10/90
ZnS:Mn	$1.36 \pm 0.43$	$2.99 \pm 0.43$	$4.45 \pm 0.16$	57–62	4/96
ZnS(Zn):Mn	$0.4 \pm 0.1$	$1.2 \pm 0.1$	$7.09 \pm 0.49$	58–62	2/98

In this table,  $d_0$ —the most probable particle size,  $d$ —average size,  $d_s$ —particle size which occupies the largest part of the micrographs area,  $D$ —coherent domain size and the ratio of cubic to hexagonal ZnS phase contribution

multi-component signal (signal 1) and the wide single line (signal 2). The signal 1 originates from  $\text{Mn}^{2+}$  isolated ions in regular lattice sites, and consists of six lines, caused by allowed transitions  $M=1/2 \leftrightarrow M=-1/2$ ,  $\Delta m=0$  (this central sextet is shown in the top of Fig. 4). The forbidden transitions between them ( $M=1/2 \leftrightarrow M=-1/2$ ,  $\Delta m=1$ ) are also visible. On both sides of the main sextet the other lines from another allowed transitions ( $\Delta M=1$ ,  $\Delta m=0$ ) are observed. For the analysis of the signal and determination of paramagnetic centers parameters, the

spin-Hamiltonian, that takes into account the electronic and Zeeman nuclear interaction, as well as the fine and hyperfine structure of the spectra, was used [19, 20]. It has been found that the spectra are described by the parameters  $g=2.0025 \pm 0.0002$ ,  $A=(-62.9 \pm 0.2) \times 10^{-4} \text{ cm}^{-1}$ ,  $b_2^0=(-105 \pm 3) \times 10^{-4} \text{ cm}^{-1}$ , coinciding with the previously defined parameters of  $\text{Mn}^{2+}$  ions in the ZnS powders [21]. Obtained parameters allow assigning the signal 1 to  $\text{Mn}^{2+}$  in the lattice sites ( $\text{Mn}_{\text{Zn}}$ ) in hexagonal ZnS. The amplitude intensity of signal 1, determined using

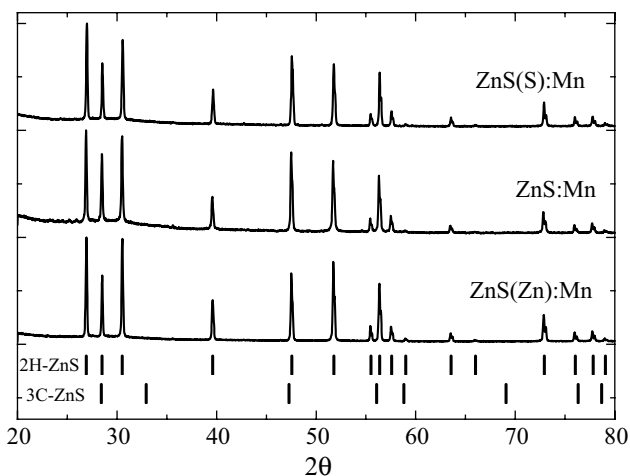


**Fig. 3** XRD patterns of ZnS(S):Mn, ZnS:Mn and ZnS(Zn):Mn and standard stick patterns for 3C- and 2H- structures of ZnS

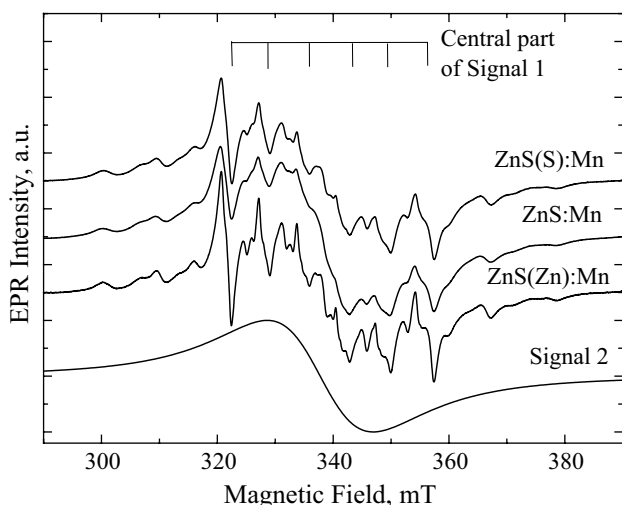


**Fig. 4** EPR spectra of ZnS:Mn, synthesized at various ratios of Zn and S in the charge

the low- field line of the central sextet, is maximal for ZnS(Zn):Mn and minimal for ZnS:Mn. It should be noted, that the form of high-field line in the central sextet is different in different samples. Most likely, this is due to the superposition of the signals from Mn<sup>2+</sup> in the cubic and hexagonal sites in different proportions. The broadening of the lines due to Mn<sup>2+</sup> dipole–dipole interaction makes hampers the accurate analysis. However, rough estimation of the line shape indicates a contribution of manganese ions in cubic lattice sites to the signal 1.

The EPR signal similar to the signal 2 was often observed in studies, devoted to the highly doped ZnS:Mn, (for example, in [22, 23]). Its nature will be discussed below.

The integral EPR intensity ( $I_{EPR}$ ), calculated as the double integral of the experimental spectrum, differs in all investigated samples. So,  $I_{EPR}^{ZnS(S):Mn}/I_{EPR}^{ZnS:Mn}/I_{EPR}^{ZnS(Zn):Mn} = 3.3/3.9/1.5$ . It is obvious that the signal 2 gives the main contribution to the EPR spectrum. The number of paramagnetic centers evaluated from integral EPR spectra exceeds slightly the value expected for 1 wt% of Mn doping.

### 3.2 Optical characteristics

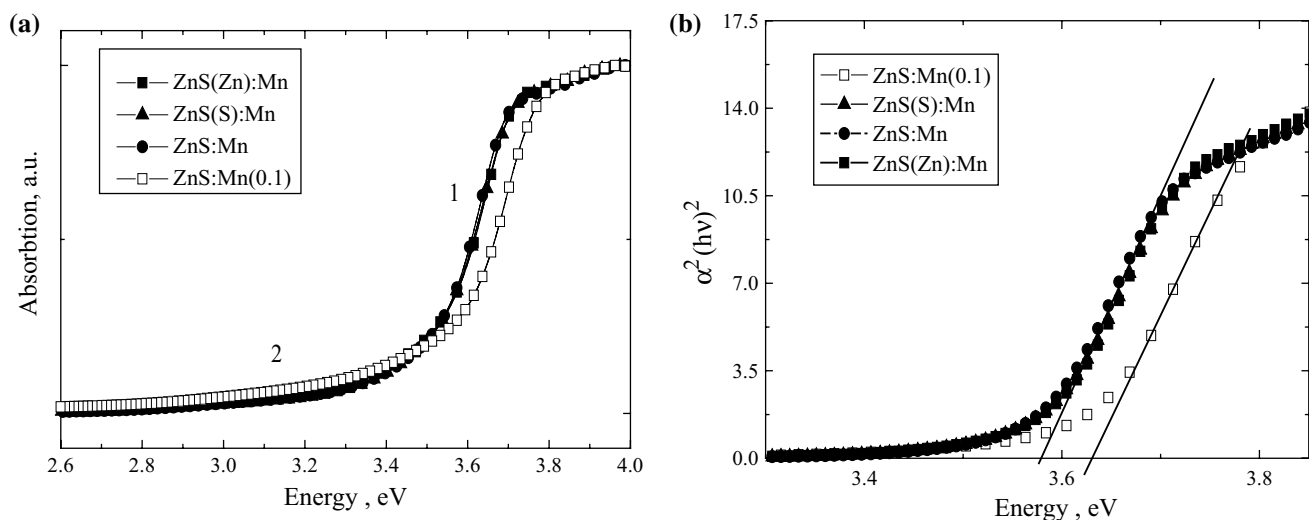
#### 3.2.1 Study of the absorption edge

Figure 5 shows the absorption spectra and the dependence  $\alpha^2(h\nu)^2$  on  $h\nu$  of the investigated powders, obtained by converting the diffuse reflection spectra using the standard program based on the Kubelka–Munk ratio  $f(r_\infty) = \frac{(1-r_\infty)^2}{2r_\infty} = \frac{K}{S}$ , where  $f(r_\infty)$ —Kubelka–Munk function,  $r_\infty = R_{sample}/R_{BaSO_4}$ —relative diffuse reflection from the sample, K and S—absorption and scattering coefficients of the sample, respectively.

Besides the absorption spectra of the powders, synthesized at various ratios of zinc and sulfur in the charge, containing 1 wt% Mn, Fig. 5 also shows the spectra of ZnS:Mn(0.1) powder, grown from the charge, containing stoichiometric ratio of Zn/S, and 0.1 wt% of manganese. As one can see, the fundamental absorption edge in all the samples consists of two parts (1 and 2) (Fig. 5a). One of them (part 1) is described by the dependence  $\alpha h\nu = \text{const}(E_g - h\nu)^{1/2}$  (Fig. 5b), corresponding to the fundamental absorption edge in the direct gap semiconductor. As Fig. 5 shows, the absorption spectra for ZnS(S):Mn, ZnS:Mn and ZnS(Zn):Mn with Mn 1 wt%, practically coincide. At the same time, part 1 for ZnS:Mn(0.1) is shifted to shorter wavelengths (Fig. 5a) and shows the higher  $E_g$  value (~3.63 eV) compared to other samples grown at different Zn/S ratio and doped with 1 wt% of Mn (Fig. 5b). The long-wavelength shift of the fundamental absorption edge in the Zn (S):Mn, ZnS:Mn and ZnS(Zn):Mn can be assigned, obviously, to the formation of ZnS–MnS solid solution.

#### 3.2.2 Luminescent characteristics

Figure 6a represents photoluminescence spectra of the investigated powders at a high level of excitation. All spectra have well revealed three bands with maxima in the region 450–465, 505–510 and 580–595 nm. It is known [24–26] that bands at 450–465 and 505–510 nm are caused by the centers of self-activated (SA) emission and are the superposition of several bands. The variation of stoichiometry of undoped ZnS crystals was shown to result in the



**Fig. 5** The absorption spectra (a) and dependence  $\alpha^2(h\nu)^2$  via  $h\nu$  (b) of the investigated powders

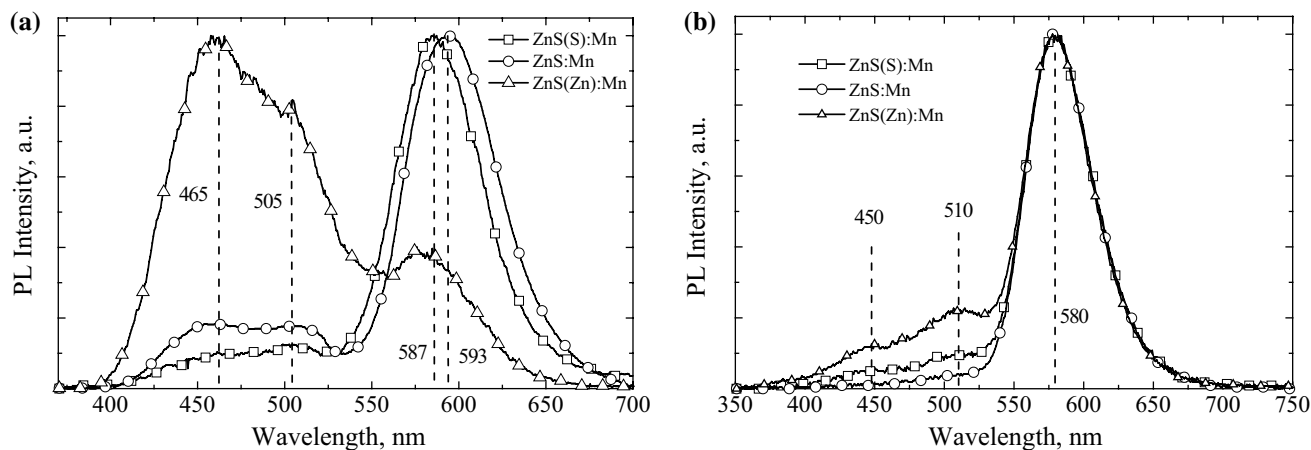


**Fig. 6** PL spectra of ZnS:Mn samples at excitation wavelength of 337 nm from a nitrogen laser (a) and xenon lamp (b)

change of the contribution of the different SA-emission bands in PL spectra. In the crystals grown with an excess of Zn, the 466 nm band is dominant [27], in the case of composition, close to the stoichiometric,  $\lambda_{\max} \sim 365$  nm band is mainly observed, and in case of sulfur excess PL spectra is dominated by the 505–510 nm band. It should be noted, that the change of PL spectra in blue region, some authors [24, 25] attribute to recharging of oxygen complexes, involved in SA-luminescence, while the other ones [27] ascribe this change to the formation of intrinsic defects of various types.

The band with  $\lambda_{\max} \sim 580$ –590 nm, caused by Mn impurity, is also complicated. It consists of a set of individual bands with  $\lambda_{\max} = 557, 587, 600$  nm assigned to Mn atoms with different localization in the ZnS lattice [28–30]. The band with  $\lambda_{\max} = 600$  nm is ascribed to interstitial  $\text{Mn}^{2+}$  ions in octahedral environment, the band

with  $\lambda_{\max} = 578$  nm is assigned to  $\text{Mn}^{2+}$  ions located near the dislocations or point defects [28], and a band with  $\lambda_{\max} = 557$  nm is attributed to the  $\text{Mn}_{\text{Zn}}$ . Several authors [30] suppose the emission band with  $\lambda_{\max} = 557$  nm to be complex and caused by emission centers, which are located in the lattice sites in the cubic and hexagonal ZnS. As it can be seen from Fig. 6, the Zn/S ratio in the charge has a significant impact on PL spectra of ZnS:Mn. It affects not only the ratio of intensities of SA- and Mn-related bands, but also the contribution of different components in the SA emission spectrum.

The maximum contribution of SA-bands in the PL spectra is observed in the samples with zinc excess, the band with  $\lambda_{\max} = 466$  nm being dominant, that is consistent with the data of [27]. The minimum contribution of the self-activated photoluminescence bands is observed in the case of the sulfur excess, the band with  $\lambda_{\max} = 505$ –510 nm being

dominant in SA emission spectra, that is also consistent with data of other studies [24, 25].

As it can be seen from Fig. 6a, the changes in the charge composition also affect the spectral position of Mn-related band that indicates the dependence of Mn localization in the lattice on Zn/S ratio. The most short-wave position ( $\lambda_{\max} = 580$  nm) is observed in ZnS(Zn):Mn, which can be caused by the increase of the contribution of the band, corresponded to the  $\text{Mn}_{\text{Zn}}$  ions. At the same time, the most long-wave position ( $\lambda_{\max} = 593$  nm) is observed in ZnS:Mn that can be due to the increase of the contribution of interstitial Mn emission. The intermediate spectral position of Mn-related band in ZnS(S):Mn can be associated with the contribution of centers, located near the dislocations or point defects, whose concentration can be higher in these samples.

PL spectra at low excitation level are shown in Fig. 6b. As it can be seen, they also show three bands: two ones caused by the SA-emission centers and one band caused by manganese centers. The relationship of Mn-related and SA-bands intensities also depends on the Zn/S ratio. The maximum intensity of the SA-emission is observed in ZnS(Zn):Mn, while the minimum value was found to be in ZnS:Mn sample, which, in accordance to the EPR data, corresponds to the minimum and maximum of manganese concentration. This is in consistence with the known dependence of the SA-emission intensity on the concentration of introduced manganese.

The excitation spectra of the Mn-related emission band are represented in Fig. 7.

As it can be seen from the figure, all the spectra have five bands with maxima at  $\lambda_{\max} \sim 337\text{--}345$ , 390, 412, 467, 493 nm. The band with  $\lambda_{\max} \sim 337\text{--}345$  nm corresponds to the fundamental absorption of ZnS (intrinsic maximum). The bands with  $\lambda_{\max} \sim 390$ , 412, 467, 493 nm correspond to the known manganese absorption bands [30, 31], which are usually appear in PLE of Mn-related PL bands. It should be noted that the intrinsic maximum position in PLE spectra is different for different groups of samples. The most short-wave position corresponds to the ZnS(Zn):Mn sample, while the most long-wave position is observed in ZnS:Mn.

#### 4 Discussion

Analysis of the data provides information on the dependence of the amount of manganese embedded in the microcrystals and its spatial distribution on the Zn/S ratio.

One of the features of the investigated samples is the presence of two different Mn-related EPR signals which intensity depends on Zn/S ratio. These signals correspond obviously to the different regions in the microcrystals. The

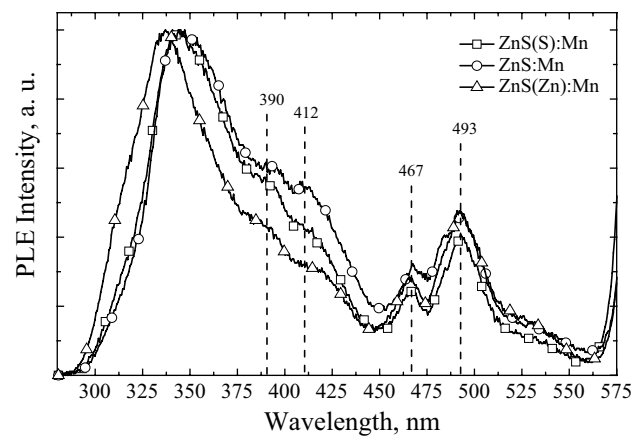


**Fig. 7** PLE of 590 nm band from ZnS:Mn powders

signal 1 caused by isolated  $\text{Mn}^{2+}$  ions in a regular lattice sites can be assigned to relatively low doped regions.

As for the signal 2, its origin is controversial. In particular, it is ascribed to  $\text{Mn}^{2+}$  ions, located in areas of their high local concentration and bounded by dipole–dipole interaction [22, 23]. As it was shown in [22], the thermal annealing of the samples resulted in a decrease of its intensity and in an enhancement of the signal 1. This indicates the possibility of Mn ions exchange between such regions with temperature increase.

On the other hand, the signal 2 can be caused by  $\text{Mn}^{2+}$  ions, which are located in areas with highly damaged structure. In this case, the interaction with the environment for the two individual ions can be very different, leading to the spread of the spin-Hamiltonian parameters for the ensemble of ions and the appearance of broad structureless line in the EPR spectra.

Besides, such a signal can be caused by clusters, which contain closely spaced Mn ions with strong exchange interaction. In the latter case, a so-called superparamagnetic system in which a cluster interacts with a magnetic field as a whole appears. Such behavior has been observed previously for Mn and Cu in highly doped CdS:Mn [32] and ZnS:Cu [33].

As it can be seen from Fig. 5b, the appearance of the signal 2 in EPR spectra is accompanied by a shift of the absorption edge to longer wavelengths (a decrease of the band gap). Therefore, it can be assumed that this signal corresponds to the solid solution. Thus, one of the reasons of its appearance may be a high Mn ions concentration in this area. However, as it is noted above, estimation of the number of paramagnetic centers in studied powders gives a somewhat higher value than it is expected at a 1% manganese doping. This can be assigned to the contribution of the superparamagnetic component into signal 2, because in this case the standard evaluation of paramagnetic center

concentration is not correct. At the same time, the presence of areas with heavily damaged structure is not clearly confirmed by the structural studies data.

Thus, ZnS doping with Mn at concentration of 1 wt% leads to formation of solid solution domains while the presence of two EPR signals indicates inhomogeneous Mn distribution. Such Mn distribution is confirmed by the decrease of the EPR spectra intensity, normalized to the weight of the sample, during the etching. Since the intensity of the EPR spectra is determined mainly by broad signal, it can be concluded that the solid solution regions are located near the surface of the microcrystals.

The obtained results indicate also that the amount of manganese incorporated in the ZnS depends on the Zn/S ratio in the charge during powder synthesis. Maximal integral intensity of the EPR signal corresponds to the sample synthesized under stoichiometry conditions while minimal intensity is observed in the sample synthesized with zinc excess. Thus, in opposite to ZnSe:Mn data obtained in [16] the chalcogen excess does not result in the best Mn incorporation. The non-monotonic dependence of the amount of incorporated manganese on Zn/S ratio apparently caused by following factors: the difference in potential barrier to its incorporation, which can explain the increase of Mn amount at  $Zn/S < 1$ , and in the difference in crystallite sizes. The latter can result in the different number of extended defects which promotes Mn diffusion in microcrystals. Indeed, the coherent domain sizes are nearly the same in the different samples while the microcrystallite sizes are different. Therefore, the maximal number of such defects is present in the samples with maximal sizes, i.e. in the samples grown under stoichiometric conditions. In this case, the maximal Mn content in these samples is obviously caused by the impurity incorporation along extended defects [34].

Investigation of the PL and PLE spectra provides information on the effect of the Z/S ratio on SA-luminescence spectra as well as on the depth distribution of Mn-related emission centers.

As follows from the data obtained, the SA and Mn-related band relative intensities depend on the Zn/S ratio. One of the reasons can be the difference in the amount of embedded Mn. Indeed, it is known [34] that when the concentration of manganese increases SA emission intensity decreases. However, in the case of a high excitation level it is not entirely consistent with the EPR data. Indeed, on the one hand the minimal total concentration of manganese (signal 2) is observed in ZnS(Zn):Mn, where the intensity of SA luminescence is maximal, which is consistent with the assumption above. On the other hand, the maximal number of EPR centers is observed in ZnS:Mn, while the minimal contribution of SA bands is observed in the other sample: namely, ZnS(S):Mn. Another reason can be

non-uniform depth distribution of the different luminescence centers. This is evidenced by PLE spectra, as well as by differences in the photoluminescence spectra at low and high excitation levels. It should be noted that this analysis provides the information on the emission center depth distribution in the near-surface region of microcrystals because the depth of excited light penetration (in the intrinsic PLE maximum) is nearly 100 nm that is of the order of coherent domain size.

As it was mentioned above, in the PLE spectra of Mn-related band, the position of its intrinsic maximum depends on Zn/S ratio. This, in principle, can be caused by the difference in the absorption spectra (shift of the fundamental absorption edge). However, as it can be seen from Fig. 5b, this difference for the ZnS(S):Mn, ZnS:Mn and ZnS(Zn):Mn samples is insignificant. Therefore, it can be assumed that the changes in the absorption spectra are not the reason of the PLE maximum shift. At the same time, the inhomogeneous depth distribution of the manganese luminescence centers in microcrystals can explain the observed difference in the PLE spectra. In this case, the closer to the surface of the microcrystals is the location of manganese centers the more short-wave position of PLE maximum will be observed. The most short-wave position takes place in ZnS(Zn):Mn, while the most long-wave one is found in ZnS:Mn, i.e. PLE maximum shifts to longer wavelengths with the increase of embedded manganese concentration. This means that the depth distribution of Mn-related luminescence centers depends on the amount of Mn embedded in microcrystals. The conclusion about the preferential localization of manganese luminescent centers in near-surface region of the microcrystals is consistent with PL spectra measured at different excitation levels. Indeed, the increase of excitation intensity results in the increase of the excited crystal thickness. If the Mn-related centers are localized near the surface, while SA-centers are present in the microcrystal volume, the contribution of Mn-related bands will be more pronounced at low excitation level than at high one. Just this is the case. Both these observations (PLE spectra and PL spectra at different excitation levels) can indicate that the manganese centers are located mainly in the near-surface region of microcrystals while SA luminescence centers are distributed more homogeneously.

Thus, the number of embedded manganese and its distribution in the depth of microcrystals depend on the Zn/S ratio. In the case of zinc excess Mn-related emission centers are located closer to the microcrystal surface than in the case of the Zn/S stoichiometric ratio.

It should be noted that the concentration and depth distribution of the own defects, responsible for SA-emission may also partly disturb the known relationship between SA and Mn-related band intensities that is observed at high excitation level.

The preferential localization of solid solution areas and manganese luminescence centers near the surface of the microcrystals can be caused by the processes of the segregation that were previously observed in ZnS crystals, synthesized by SHS method [13, 14].

## 5 Conclusions

The investigations of zinc sulfide powders, synthesized by SHS method from a charge with different ratio of Zn/S have shown that this ratio has a significant impact on the morphology (size) of the crystallites, as well as their luminescent properties. The most homogeneous size distribution, were found at stoichiometric Zn/S ratio. At the same time, the largest contribution of the small crystallites is found in powders synthesized with sulfur excess. It is shown that the microcrystals consist of nanometer blocks the size of which does not depend on the charge composition.

Besides, the following characteristics also depend on Zn/S ratio. They are cubic phase contribution, amount of embedded Mn and Mn depth distribution. It was found that cubic phase contribution increases with the increase of sulfur content in the charge. At the same time, the greatest amount of embedded Mn is observed in the powder grown at a stoichiometric Z/S ratio while the minimal value is found in the samples synthesized with the Zn excess. In addition, the concentration of Mn centers responsible for Mn-related PL bands decreases from the surface of the microcrystal to the depth. Their nearest location to the surface is observed in crystallites grown with zinc excess. It was found that when the concentration of manganese in the charge is 1%, the fundamental absorption edge is shifted to the longer wavelength that is probably caused by the formation of a ZnS–MnS solid solution with a smaller band gap.

## References

1. Y.A. Ono, *Electroluminescent displays*, (River Edge, NJ: World Scientific, Singapore, 1995)
2. J.H. Park, S.H. Lee, J.S. Kim, A.K. Kwon, H.L. Park, S.D. Han, White-electroluminescent device with ZnS:Mn, Cu, Cl phosphor. *J. Lumin.* **126**, 566–570 (2007)
3. S. Ummartyotin, N. Bunnak, J. Juntero, M. Sain, H. Manuspiya, Synthesis and luminescence properties of ZnS and metal (Mn, Cu)-doped-ZnS ceramic powder. *Solid State Sci.* **14**, 299–394 (2012)
4. B.A. Smith, J.Z. Zhang, A. Joly, J. Liu, Luminescence decay kinetics of Mn<sup>2+</sup>-doped ZnS nanoclusters grown in reverse micelles. *Phys. Rev. B* **62**, 2021–2028 (2000)
5. G. Hajisalem, M. Maradi, N. Taghavinia, M. Houshiar, The two-step thermochemical growth of ZnS:Mn nanocrystals and a study of luminescence evolution. *Nanotechnology* **20**, 095706 (2009)
6. H. Yang, J. Zhao, L. Song, L. Shen, Z. Wang, L. Wang, D. Zhang, Photoluminescent properties of ZnS:Mn nanocrystals prepared in inhomogeneous system. *Mater. Lett.* **57**, 2287–2291 (2003)
7. R.N. Bhargava, D. Gallagher, X. Hong, A. Nurmikko, Optical properties of manganese-doped nanocrystals of ZnS. *Phys. Rev. Lett.* **72**, 416–419 (1994)
8. A. Jrad, W. Naffouti, T.B. Nasr, S. Ammar, N. Turki-Kamoun, J. Mater. Sci. (2016). Doi:10.1007/s10854-016-5682-z
9. S.T. Arunaa, A.S. Mukasyan, Combustion synthesis and nanomaterials. *Curr. Opin. Solid State Mater. Sci.* **12**, 44–50 (2008)
10. A.A. Borisov, L. De Luca, A. Merzhanov, *Self-Propagating High-Temperature Synthesis of Materials*, ed. By B. Scheck, Combustion Science & Technology Book Series, V.5, Taylor & Francis, New York, 2002
11. J.H.S. Lee, S. Goroshin, A. Yoshinaka, M. Romano, J. Jiang, I. Hooton, F. Zhang, *Shock compression of condensed matter*, ed. By M.D. Furnish, L.C. Chhabildas, R.S. Hixton (American Institute of Physics, Melville, 2000)
12. S.V. Kozytckyy, V.P. Pysarskyy, D.D. Polishchuk, Obtaining of ZnSe by means of self-propagating high-temperature synthesis. *PCSS* **4**, 229–233 (2003)
13. B. Krupińska, Z. Rdzawski, M. Krupiński, K. Labisz, Microstructure investigations of cast Zn–Al alloys. *JAMME* **61**, 12–19 (2013)
14. S.V. Kozitsky, A.N. Krasnov, Formation “qiqantic” crystals in crystallization of ZnS. *J. Cryst. Growth* **165**, 166–168 (1996)
15. A.G. Merzhanov, A.S. Rogachev, Structural macrokinetics of SHS processes. *Pure Appl. Chem.* **64**, 941–953 (1992)
16. S.C. Erwin, L. Zu, M.I. Haftel, A.L. Efros, T.A. Kennedy, D.J. Norris, Doping semiconductor nanocrystals. *Nat. Lett.* **436**, 91–94 (2005)
17. G.M. Dalpian, J.R. Chelikowsky, Self-purification in semiconductor nanocrystals. *Phys. Rev. Lett.* **96**, 226802 (2006)
18. M. Rubenstein, Zn-rich liquids of Zn-S system between 1000 and 1300 °C. *J. Crystal. Growth* **41**, 311–316 (1977)
19. S.A. Altshuler, B.M. Kozyrev, *Electron paramagnetic resonance in compounds of transition elements*. (Nauka, Moscow, 1972), p. 670
20. C. Rudowicz, S.K. Misra, Spin-Hamiltonian formalisms in electron magnetic resonance (EMR) and related spectroscopies. *Appl. Spectrosc. Rev.* **36**, 11–63 (2001)
21. I.P. Vorona, V.G. Grachev, S.S. Ishchenko, N.P. Baran, Yu.Yu. Bacherikov, A.G. Zhuk, V.V. Nosenko, Structure study of low-dimensional ZnS powders using EPR of Mn<sup>2+</sup>. *Ions. Appl. Spectr.* **3**, 60–65 (2016)
22. N.E. Korsunskaya, Yu.Yu. Bacherikov, T.R. Stara, V.P. Kladko, N.P. Baran, Yu. O. Polishchuk, A.V. Kuchuk, A.G. Zhuk, Ye.F. Venger, Features of ZnS-powder doping with a Mn impurity during synthesis and subsequent annealing. *Semiconductors* **47**, 713–720 (2013)
23. T.H. Yeom, Y.H. Lee, T.S. Hahn, M.H. Oh, Electron-paramagnetic-resonance study of the Mn<sup>2+</sup> luminescence center in ZnS:Mn powder and thin films. *J. Appl. Phys.* **79**, 1004–1007 (1996)
24. N.K. Morozova, D.A. Mideros, N.D. Danilevich, Absorption, luminescence excitation, and infrared transmittance spectra of ZnS(O)–ZnSe(O) crystals in the context of the band anticrossing theory. *Semiconductors* **43**, 162–167 (2009)
25. N.K. Morozova, I.A. Karetnikov, V.V. Blinov, E.M. Gavrichuk, A study of luminescence centers related to copper and oxygen in ZnSe. *Semiconductors* **35**, 24–32 (2001)
26. N.D. Borisenko, V.I. Klimenko, B.A. Polezhaev, Effect of the excitation mode on the emission spectrum of manganese in zinc sulfide. *Zh. Prikl. Spektrosk.* **50**, 475–477 (1989)
27. J.E. Nicholls, J.J. Davis, B.C. Cavenott, Spin-dependent donor-acceptor pair recombination in ZnS crystals showing the self-activated emission. *J. Phys. C* **12**, 361–379 (1979)

28. N.D. Borisenko, B.A. Polezhaev, Lifetime of excited Mn states in zinc sulfide. *Zh. Prikl. Spektrosk.* **53**, 1020–1022 (1990)
29. H.-E. Gumlich, Electro- and photoluminescence properties of Mn in ZnS and ZnCdS. *J. Lumin.* **23**, 73–99 (1981)
30. M.F. Bulanyi, B.A. Polezhaev, T.A. Prokof'ev, I.M. Chernenko, Excitation spectra and structure of luminescence centers of manganese ions in single crystals of zinc sulfide. *Appl. Spectrosc.* **67**, 282–286 (2000)
31. V.F. Agekian, Intracenter transitions of iron-group ions in II-VI semiconductor matrices. *Phys. Solid State* **44**, 2013–2030 (2002)
32. G. Counio, S. Esnouf, T. Gacoin, J.-P. Boilot, CdS:Mn nanocrystals in transparent xerogel matrices: synthesis and luminescence properties. *J. Phys. Chem.* **100**, 20021–20026 (1996)
33. Yu.Yu. Bacherikov, I.P. Vorona, A.A. Konchits, S.V. Optasyuk, S.V. Kozitskiy, K.D. Kardashov, The paramagnetic and luminescence properties of single-stage synthesized ZnS:Cu. *Funct. Mater.* **17**, 158–163 (2010)
34. Yu.Yu. Bacherikov, S.V. Optasyuk, Diffusional relaxation in ZnS after thermal doping at 800 °C. *Appl. Spectrosc.* **77**, 95–103 (2010)